Chapter-5

Fluorescent CNDs from ethanolic extract of Andrographis paniculata and their applications

5.1 Introduction

Photomedicine is an interdisciplinary science that studies the effects of light on human health as well as the role of light in disease detection, diagnosis, and treatment [Hamblin *et al*., 2013]. Because the surface area to mass ratio of nanomaterials is higher than that of macroscopic materials, the light-matter interaction is more robust in nanomaterials [Hamblin *et al*., 2015]. Quantum dots, plasmon resonance, and gold nanoparticles with adaptable absorption spectra have controllable optical properties, demonstrating a size-wavelength relationship that gives these nanomaterials multifunctionality. As discussed in Chapter **1**, carbon nanodots (CNDs) are carbon nanostructures with a diameter of 1–10 nm that exhibit tunable fluorescence without being much toxic [Zhang *et al*., 2018]. CNDs are ideal photomedicine because of their photobleaching resistance, tunable optical properties, inert chemical and biocompatible nature, simple functionalization, and photoluminescence [Kang *et al*., 2020].

Botanical extracts, phytopharmaceuticals, and their isolated phytoconstituents are referred to as phytomedicines and are responsible for inducing pharmacodynamic effects [Bonam *et al*., 2018]. Photoactive phytoprinciples are abundant in nature and can be found in various plant extracts [Khan *et al*., 2019]. These phytomedicines have been the foundation for pharmacological treatments since dawn. People in rural areas still rely on them for primary healthcare and palliative care [Siewert *et al*., 2019].

Phytomedicines and their chemical scaffolds have a long history as essential starting points for drug discovery and structural modifications of various modern medicines. *Andrographis paniculata* (AP), among other phytomedicines, has a long history in southern and southeast Asian traditional medicine systems. Because of its exceptional medicinal properties against carcinomas, liver disorders, diabetes, and various inflammatory infections, AP has been used worldwide [Dai *et al*., 2019].

Cancer is defined as the uncontrolled proliferation of cells in the body, which leads to life-threatening situations [Cox *et al*., 2021]. Breast cancer is a common heterogeneous carcinoma in women worldwide, and it is curable in 70-80% of patients in their early stages. Malignant breast cancer is notoriously resistant to the current crop of chemotherapeutics. Breast cancer is heterogeneous, involving mutations in the BRCA (tumor suppressor gene), activation of the HER2 (human epidermal growth factor receptor), and hormone receptors (estrogens and progesterone receptors) on the molecular level [Harbeck *et al*., 2019]. CNDs make bio-labeling of cancer cells easier, making a timely diagnosis of various carcinomas possible, which allows for effective cancer management and quick recovery [Zhang *et al*., 2018]. These CNDs have minimal toxic effects and *in-vivo* stability, as well as cost-effectiveness and biocompatibility for successful bio-labeling [Atchudan *et al*., 2018]. Cherenkov luminescence imaging, fluorescence tomography, *in-vivo* confocal microscopy, photoacoustic techniques, and optical frequency domain imaging are some of the sophisticated optical methodologies based on the luminescence phenomenon that is widely used in healthcare [Gul *et al*., 2019]

EAPCDs (Ethanolic extract of *Andrographis paniculata* derived carbon dots) were synthesized using ethanolic *Andrographis paniculata* leaves extract as a carbon, nitrogen and sulfur source in this study. EAPCDs can be used as important photomedicine in a variety of medical settings. There are several examples of phytomedicines being used as a photomedicine, such as the ancient Egyptians and Persians treating skin diseases by consuming various plants and then exposing themselves to sunlight. Most synthesized CNDs have been reported in the short wavelength region. However, there is a considerable need to develop long-wavelength CNDs because they have better biological and physicochemical properties [Huang *et al*., 2019, Zhan *et al*., 2018]. CNDs were investigated for their size morphology, surface properties, chemical properties, optical properties, and thermal stability. These CNDs had a distinct pink fluorescence, which was noticeable compared to previous reports. This is the first report we are aware of on developing pink fluorescent CNDs derived from phytomedicine using a one-pot synthesis method. EAPCDs' role in metal sensing, cancer cell bioimaging, viability studies using MDR strains of bacteria, free radical sensing, and scavenging are discussed.

5.2 Experimental section

5.2.1 Authentication of plant and extraction

Andrographis paniculata leaves were collected at the Indian Institute of Technology (BHU) campus in Varanasi, Uttar Pradesh, India. Taxonomist Prof. N.K. Dubey certified the plant specimen, which was then deposited in the herbarium of the Department of Botany, Banaras Hindu University, Varanasi, with the specimen number

Acantha. 2020/1 for future reference. The plant was also authenticated using the DNA fingerprinting technique with the matK gene. Fresh AP leaves 10 g of were washed in distilled water, dried thoroughly to remove moisture, and then subjected to maceration with 150 mL ethanol until the volume was reduced to 100 mL for the preparation of ethanolic extract (EEAP).

5.2.2 Fabrication of EAPCDs

CNDs were fabricated by hydrothermal treatment of an ethanolic extract of fresh *Andrographis paniculate* leaves (EEAP). CNDs were made by heating EEAP to 160^0C for 8 h in a teflon-lined hydrothermal autoclave and were then centrifuged at 11000 rpm for 15 minutes. A membrane syringe filter (0.22 µm) was used to purify the CNDs further. EAPCDs stands for ethanolic extract-derived CNDs, while EEAP stands for ethanolic *Andrographis paniculata* leaves extract. EAPCDs were stored at 4°C for further characterizations and biological evaluations.

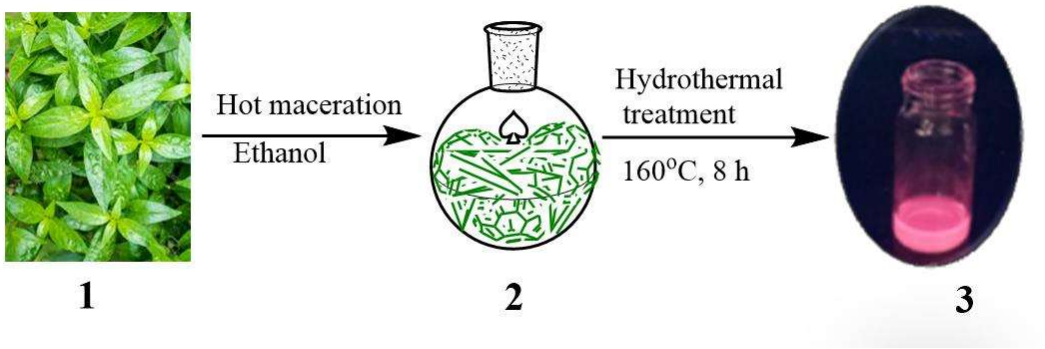

Scheme 5.1 Synthesis of pink fluorescent carbon nanodots (3) via the hydrothermal treatment of ethanolic extract (2) of fresh leaves of *Andrographis paniculata* (1).

5.2.3 Characterization, optical properties, and stability studies of EAPCDs

The fabricated CNDs have been characterized to study their morphology, fluorescence properties, surface functional groups, crystallinity, elemental composition, stability, and quantum yield using different techniques. The detailed procedures are provided in chapter **3**.

5.2.4 Applications of EAPCDs

5.2.4.1 Sensing of environmentally and biologically relevant metal ions

The metal ion sensing ability of the EAPCDs was evaluated as per the previously reported methods with certain modifications [Edison *et al*., 2016]. The detailed procedures for metal sensing by EAPCDs are provided in chapter **3**.

5.2.4.2 Cytotoxicity studies and cellular imaging of EAPCDs

MTT assay was carried out as per the previously reported methods with certain modifications [Pandey *et al*., 2020] using different concentrations of EAPCDs (0, 0.1, 0.2, 0.5, 0.7, 1, 1.5, 2.0, 2.5, 3.0 mg/ mL) employing MCF-7 breast cancer cells. Other details have been provided in Chapter **3**. For cellular imaging, MCF-7 cells were seeded at a density of 5×10^6 cells per well in a 6-well plate. The cells were then grown for 24 h in a 5% CO_2 humidified incubator at 37 ^{0}C and were then incubated for another 24 h after being treated with EAPCDs (0.7 mg/mL). The cells were washed three times with 1X PBS before being fixed in 4% paraformaldehyde for 30 minutes before being imaged. EVOS invitrogen fluorescence microscopy (Life technologies) was used for *in-vitro* cellular imaging.

5.2.4.3 Viability studies using multi drug-resistant bacterial culture

The viability of MDR clinically isolated strains of *Staphylococcus aureus* (G+) and *Klebsiella pneumonia* (G-) was tested using the disc diffusion method [Torkian *et al*., 2022] with minor modifications with EAPCDs (50µL of 6 mg/mL). Other details have been provided in Chapter **3**.

5.2.4.4 Free radicals sensing and scavenging potential

The radical scavenging ability of EAPCDs at different concentrations of 240 µg/mL, 480 µg/mL, and 960 µg/mL was determined using a modified DPPH assay [Sheng *et al.*, 2022]. The detailed procedures for the free radical scavenging potential of CNDs are provided in chapter **3**.

5.2.4.5 In-vivo toxicity evaluation

CNDs are expected not to induce severe adverse effects in animals to be used in therapeutic settings. Ethical treatment and housing conditions are provided in Chapter **3**, section. On day 0, the EAPCDs were dispersed in PBS to make a dispersion with the concentration of 0.7 mg/kg BW and administered intraperitoneal injection. Mice in the control group were administered with PBS. All experimental animals survived the experiment, and their body weight changes were identical to those of the control group. On the 14th day, blood was obtained from the mice, and routine biochemical and hematological assays were done as described in chapter **3**.

5.2.5 Statistical analysis

The data is presented as Mean± Standard Deviation (SD). One-way ANOVA was used to perform the statistical studies (GraphPad Prism Version 5.0). $p < 0.05$ was considered as a criterion for significance.

5.3 Results and Discussion

5.3.1 Formation of EAPCDs

Andrographolide, 14-deoxyandrographolide, chlorophyll, amino acids, sugars, -sitosterol, 5,2'- dihydroxy-7,8-dimethoxyflavone, long-chain trans-cinnamate esters, monogalactosyl diacylglycerols, triacylglycerols, and other nitrogen and sulfur-containing phytoconstituents and biological macromolecules [Dai *et al*., 2019]. Long-wavelength shifts, or pink shifts in photoluminescence, may be caused by increasing the amount of graphitic nitrogen and sulfur in the CNDs structure [Hola *et al*., 2017]. EAPCDs had a distinct pink fluorescence that was noticeable compared to previous literature reports [Pal *et al.,* 2018, Sachdev *et al.,* 2015, Qian *et al*., 2018]. It is possible to adjust their photoluminescence, spectral properties, optical properties, compositions, and structures due to changes in the electron density of CNDs systems with the help of nitrogen (N) and sulfur (S) doping, thereby expanding their applications [Sun *et al*., 2015]. Due to the different types of surface states and a wide distribution of different energy levels, doped CNDs have different physicochemical and biological properties than undoped CNDs [Lu *et al*., 2015]. Graphitic nitrogen is also responsible for midgap states within the undoped HOMO-LUMO gap, which may be responsible for pink

fluorescence at the visible spectrum's high wavelength end [Huang *et al*., 2019]. According to these findings, graphitic nitrogen, combined with the tuning of the surface chemistry of CNDs with complementary functional groups, is a critical factor that can lead to a long wavelength (pink) shift in CND's luminescence [Zhan *et al*., 2018]. They are most likely formed through hydrolysis and decomposition, followed by aromatization and condensation after passivation [De *et al*., 2014; Lim *et al*., 2015]. CNDs at 6.0 mg/mL concentration were present in the EAPCDs solution.

5.3.2 Characterization of EAPCDs

HR-TEM was used to determine the morphology of EAPCDs. Bright-field images are rarely distinguishable, as shown in Figure **5.1 a**, due to the low contrast between CNDs and TEM grids, as well as their amorphous nature and small size. They are uniform in size, with an average diameter of 2.2±0.2nm and a size range of 2–2.4nm. The SAED pattern (Figure **5.1 b**) suggests that EAPCDs are amorphous, with a diffused halo pattern devoid of rings. Diffraction peaks at 2Θ of 28.03°, 40.29°, 50.04°, and 58.78°, which correspond to crystal planes (002), (100), (102), and (103), were discovered in the X-ray diffraction pattern of EAPCDs (Figure **5.1 c**) [Chunduri *et al*., 2016]. The first three peaks correspond to graphite (sp^2) and the last one to diamond (sp^3), both of which are carbon materials. For the (103), (102), (100), and (002) planes, the d-spacing was 0.18, 0.20, 0.22, and 0.31 nm, respectively, which is equivalent to graphitic lattice spacing [Chunduri *et al*., 2016]. FT-IR spectrum was used to analyze the chemical structure of EAPCDs. At about 3402cm^{-1}, the FT-IR spectrum of EAPCDs (Figure **5.1 d**) revealed a broad and distinct OH and NH vibration mode. Peaks at 1078

cm^{-1} and 1035 cm^{-1} represented stretching and bending vibrations of C-O bonds in carboxyl groups, respectively, while peaks at 2928 cm^{-1} and 1440 cm^{-1} represented C-N and C-H stretching vibration modes.

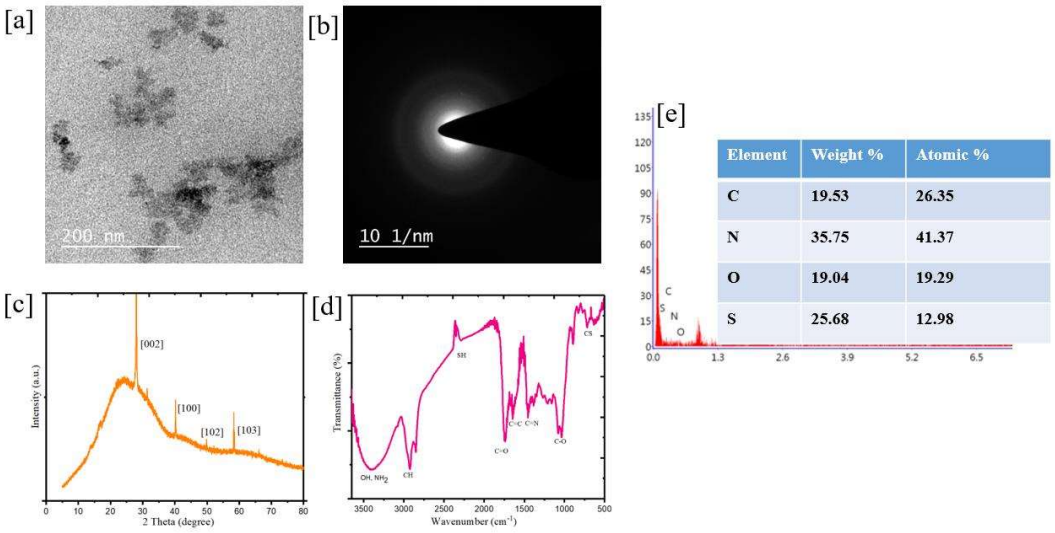

Element	Weight %	Atomic %
C	19.53	26.35
N	35.75	41.37
O	19.04	19.29
S	25.68	12.98

Figure 5.1. Characterization of EAPCDs [a] HR-TEM micrograph [b] Selected area electron diffraction (SAED) patterns [c] XRD pattern [d] FT-IR Spectrum and [e] Energy dispersive X-ray analysis (EDX) spectrum of EAPCDs.

The C-S group is responsible for the absorption at around 715 cm^{-1}. Carbon (19.53%), nitrogen (35.75%), sulfur (25.68%), and oxygen (19.04%) were the most abundant elements in EAPCDs, according to EDS elemental distributions as shown in Figure **5.1 e**. This is owed to functional groups' surface allocation.

5.3.3 Optical properties of EAPCDs

Photoluminescent carbon cores are created after aromatic centers are identified. The CNDs fluorescence behavior could be explained by the surrounding chemical moieties - carbon core interaction in conjugation with hybridization [Zhu *et al.,* 2015]. Since photoluminescence is linked to the surface character of CNDs, surface functionalization is regarded as a critical parameter [Dimos *et al*., 2016]. By occupying non-zero band gaps, the CNDs demonstrate fluorescence emission and quantum confinement effects. An infinite Bohr diameter in the excitons can explain their fluorescence mechanism [Zhu *et al.,* 2015, Wang *et al*., 2015]. The excitation max value was discovered at 455 nm using excitation spectra. When EAPCDs were exited at 455 nm, they fluoresced brightly.

Figure **5.2 a** shows excitation and emission spectra of EAPCDs, The emission wavelength ranges of 575–630 nm, with the maximum at around 600 nm. Photoluminescent spectra (Figure **5.2 b**) show a characteristic emission spectrum at various EAPCD concentrations. Optical selection of various surface defect states close to the fermi level of CNDs is the cause of this occurrence. Figure **5.2 c** shows the UV-vis absorption spectrum of EAPCDs, which shows three absorption peaks at 265 nm, 410 nm, and 665 nm wavelengths. They corresponded to the aromatic ring's π-π* transition, n-π* transitions, and n-π* transitions, respectively. The carbonic core center has a 265nm absorption peak, while the surface or molecule center has a 410nm absorption peak. In synthesized CNDs, the extended system of conjugated bonds causes the molecule to absorb visible light.

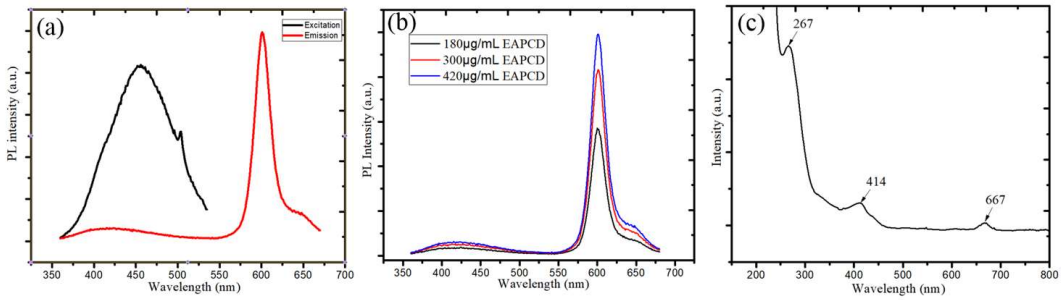

Figure 5.2. [a] Fluorescence excitation and emission spectra of EAPCDs [b] Concentration dependent fluorescence spectra of EAPCDs [c] Absorption spectrum of EAPCDs.

5.3.4 Stability studies of EAPCDs

As depicted in Figure **5.3 a**, when these CNDs were irradiated under UV at different time intervals up to 120 min, they were photostable. The TGA curve (Figure **5.3 b**) under controlled conditions demonstrated the thermal behaviour of EAPCDs, indicating weight loss as a function of temperature. TGA spectrum showed three-step degradation patterns under nitrogen atmosphere and 10°C/min heating rate.

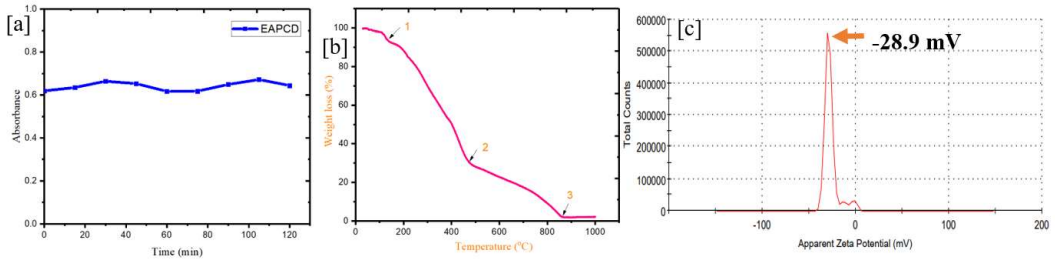

Figure 5.3. Stability studies of EAPCDs [a] Photostability study under UV illumination at a different time interval up to 120 min [b] Thermo gravimetric analysis spectrum [c] Zeta potential of EAPCD.

At 127°C, a 5.46% weight loss was observed, which can be attributed to the loss of H_2O and other molecules with weak hydrogen bonds. At 472°C, a significant 69.47% weight

loss was observed, while at 850°C, a significant 97.61% weight loss was observed. This could be due to the steady degradation or loss of the surface functional groups of EAPCDs, which indicate thermal stability up to 900°C. [Mewada *et al.,* 2013, Mehta *et al*., 2014]. Beyond 900°C, the curve flattened out. As shown in Figure **5.3 c**, EAPCDs had a ZP of -28.9 mV. The presence of negative charges on the surface of the EAPCDs causes them to repel each other, preventing particle aggregation. Due to the repellent columbic force, the synthesized CNDs may remain stable for several months, avoiding the use of pernicious surfactants. Nanoparticles with ZP values ranging from -30 mV to +30 mV have sufficient repulsive forces to achieve improved stability.

5.3.5 Applications of EAPCDs

EAPCDs have demonstrated utility in various biomedical and pharmaceutical domains such as metal sensing, cytotoxic potential, free radicals scavenging, and viability studies using MDR bacterial strains.

5.3.5.1 *Metal sensing*

With the onset of the industrial revolution, the incidences of heavy metal toxicity have also been on a surge and affecting the quality of life of people, so it is the need of the hour to devise accurate and cost-effective Hg^{2+} detection methods. In the European Union and the USA, the maximum contamination limit for Hg^{2+} is 1 ppb and 2 ppb, respectively [Fu *et al*., 2016]. Hg^{2+} as such, has no biological function in the body and is also responsible for inducing toxicity through oxidative damage and bioaccumulation. Through this objective, we found that EAPCDs can be employed to

analyze the safety and quality of drinking water by quantifying the concentration of Hg^{2+} ions.

Selectivity is a critical criterion for evaluating a CNDs ' performance. Thus, we investigated the differences in fluorescence emission intensity by adding various biologically and environmentally relevant metal ions to EAPCDs at a concentration of 250 μM, including Hg^{2+}, Fe^{3+}, Ba^{2+}, Cu^{2+}, Ca^{2+}, K^{+}, Na^{+}, NH^{4+}, As^{3+}, Bi^{3+}, and Pb^{2+} obtaining the corresponding fluorescence emission spectra as depicted in Figure **5.4 a**. Hg^{2+} had the most considerable propensity to quench the fluorescence intensity of EAPCDs among the metal ions, which can be due to the nitrogen element on the EAPCD's surface [Venkateswarlu *et al.,* 2018]. As indicated in Figure **5.4 b**, a sensitivity titration was performed under various Hg^{2+} concentrations ranging from 0 to 160 μM, and the fluorescence intensity of EAPCDs gradually decreased upon the increase in Hg^{2+} concentrations.

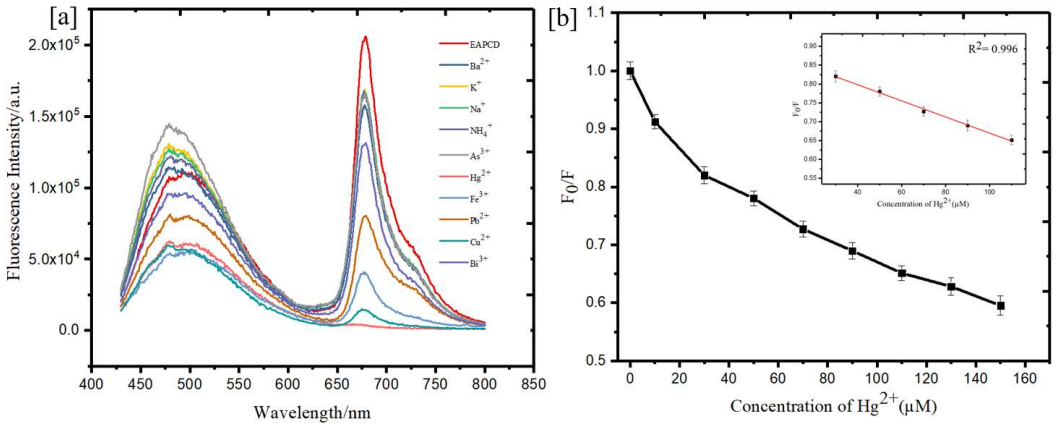

Figure 5.4. Fluorescence sensing of metal ions using EAPCDs. [a] Fluorescence responses of EAPCDs toward various metal ions. The control represents the fluorescence response of the CNDs without any ion. [b] Fluorescence responses of the EAPCDs in the presence of different concentrations of Hg^{2+}.

The electronic structure of EAPCDs is probably altered upon coordination interaction between EAPCDs and Hg^{2+} ions, which further modifies the excitons distribution and facilitates non-radiative electron-hole recombination annihilation [Xavier *et al*., 2018]. This leads to fluorescence quenching of EAPCDs. As demonstrated in Figure **5.4 b**, a good linear relationship was obtained with a correlation coefficient (R^2) of 0.996 for EAPCD with LOD=0.26 µM.

5.3.5.2 Cytotoxicity and bioimaging studies

The cytotoxicity of EAPCDs was assessed using the previously reported MTT assay with minor modifications, which used a human breast carcinoma cell line as a model. To investigate cell viability, these cells were exposed to various concentrations of EAPCDs. The findings suggested that EAPCDs have low cytotoxicity up to a specific dose, as cells were nearly 50% viable at 0.7 mg/mL (Figure **5.5 a**). In contrast to the non-treated MCF-7 cells, the cell morphology appeared distorted, and apoptotic-like changes were visible in the bright field image (Figure **5.5 b**). Between 0 and 0.5 mg/mL of EAPCDs, significant cell viability was observed, but as the dose was increased, cytotoxic effects on cells were observed. As a result, EAPCDs can be effectively used as photomedicine to inhibit cancerous growth at higher doses; however, more detailed studies are needed. Figure **5.5 b** shows a fluorescent image of MCF-7 cells that have been incubated with EAPCDs. In contrast to control cells without EAPCDs labeling, where no fluorescence was detected, the fluorescence signal was observed in the red spectral region, as shown in Figure **5.5 b**.

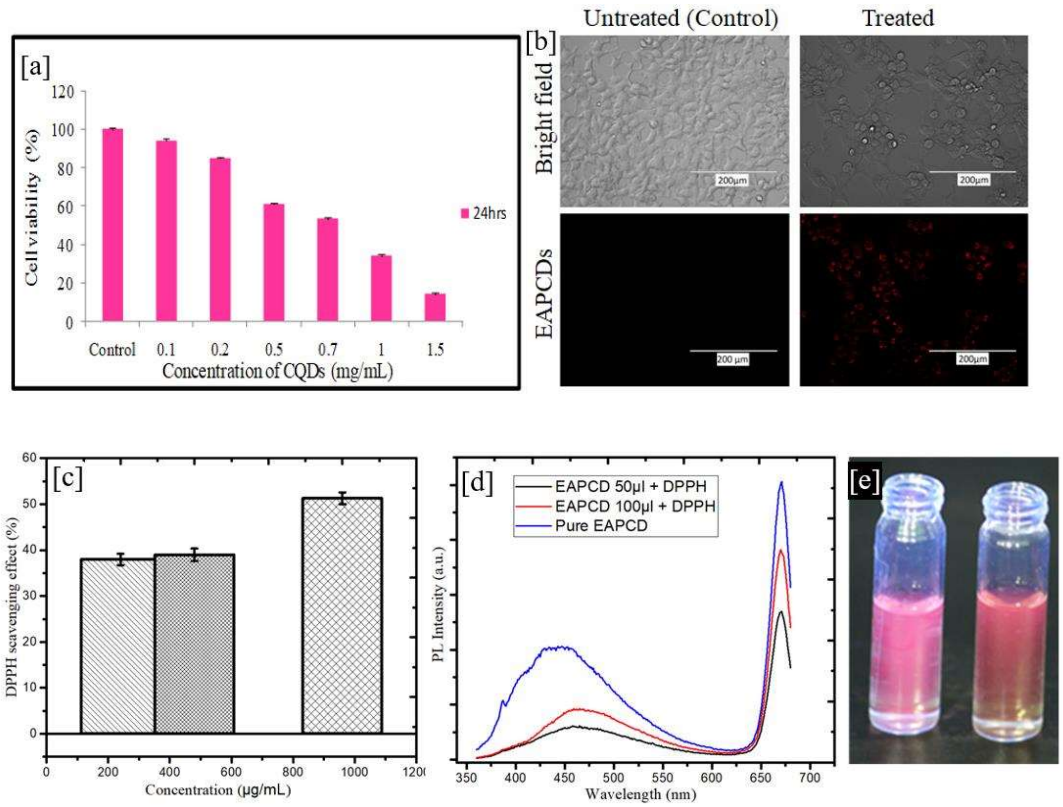

Figure 5.5. [a] MTT assay: MCF-7 cells after 24 h incubation with EAPCDs [b] *In-vitro* imaging of MCF-7 cells after 24 h of EAPCDS treatment under a bright field and red field (EAPCDs). [Scale bar: 200 µm]. [c] (%) DPPH scavenging capability of EAPCDs at different concentrations (960, 480 and 240 µg/mL) [d] EAPCDs emission spectrum displaying fluorescence quenching following free radicals addition [e] EAPCDs solution in absence of DPPH (left) and presence of DPPH (Right).

5.3.4.3. Scavenging and sensing of free radicals

Free radical sensing and scavenging capability of EAPCDs was evaluated using the DPPH assay. After forming a stable DPPH-H complex, the color of the solution changed from deep violet to light yellow. At 515 nm, absorbance was compared to a blank to determine residual DPPH. As shown in Figure **5.5 c**, increasing the dose of

EAPCDs, DPPH scavenging effect (%) enhanced. The EAPCD's fluorescence was also effectively quenched after being added to methanolic DPPH solution, as evidenced by the photoluminescence spectrum. As a control, no fluorescence quenching was observed after adding methanol. The fluorescence quenching is caused by FRET, or nonradioactive resonance energy transfer, and strong hydrogen bonding between DPPH and EAPCDs [Lin *et al*., 2012]. EAPCDs could thus be promoted as a photomedicine for detecting free radicals. The breaking or recombination of the quenchers, which occurs due to the combined effect between surface functional groups of CNDs and the target free radical, causes fluorescence quenching, as shown in Figure **5.5 c** and Figure **5.5 d**. The interaction between DPPH and the surface of the EAPCD caused the fluorescence to be quenched when DPPH was added [Huang *et al*., 2019].

5.3.5.4 Viability studies using MDR bacterial strains

The antibacterial potential of EAPCDs against two clinically isolated bacterial strains, *S. aureus* (G+) and *K. pneumoniae* (G-), was investigated in this study. The antibacterial activity of EAPCDs was investigated using the disc diffusion method with minor modifications. It was interesting to see the zones of growth inhibition of *K. pneumonia* and *S. aureus* cells around the discs added with 50 µL of 6 mg/mL EAPCDs, as shown in Figures **5.6 a** and **5.6 b**. The zone of growth inhibition of *K. pneumonia* and *S. aureus* cells was insignificant in the controlled wells containing EEAP. In contrast, the average radial diameter of the zone of growth inhibition of *K. pneumonia* and *S. aureus* was 13.4 mm and 9.2 mm, respectively, for discs containing EAPCDs. For both *S. aureus* (G+) and *K. pneumoniae* (G-), the MIC values of these CNDs were 46 µg/mL.

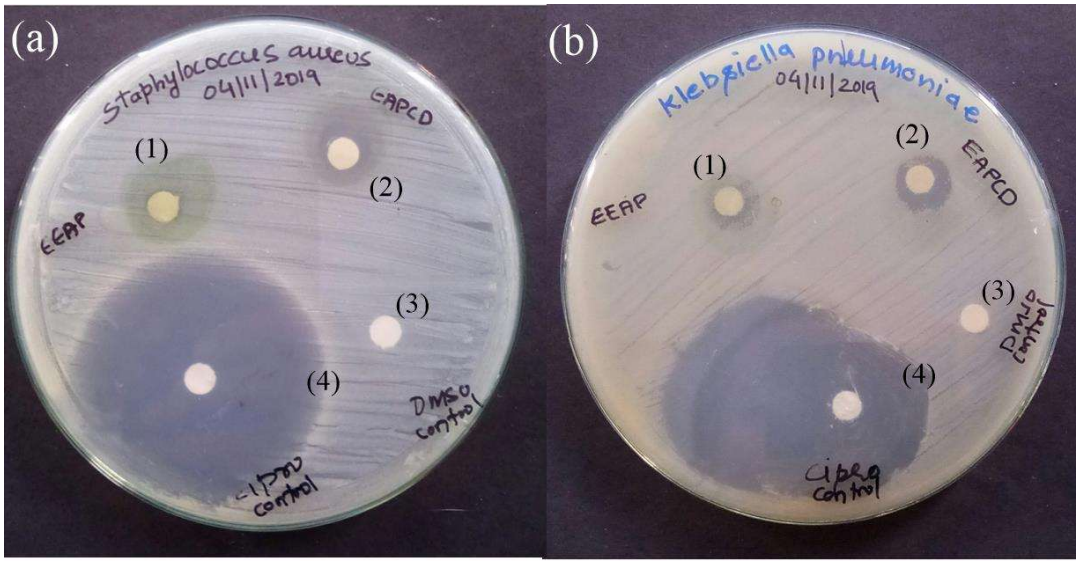

Figure 5.6. Anti-bacterial activity of EAPCDs against [a] *S. aureus*(+) and [b] *K. pneumonia*(-). (1) EEAP represents AP leaves extract, (2) EAPCDs represent AP extract-derived CNDs, (3) DMSO as a control, and (4) ciprofloxacin as a positive control.

CNDs can rupture the membrane or produce oxidizing species and free radicals that cause bacterial cells to die due to their high surface-to-volume ratio and small size [Hajipour *et al*., 2012]. Although this research lays the groundwork for developing EAPCDs as an antimicrobial photomedicine, more comprehensive in-vivo studies are needed.

5.3.5.5 In-vivo toxicity evaluation in Swiss albino mice

The results showed no evident differences between EAPCDs and control groups. Statistically insignificant ($p>0.05$) differences were observed on day 14 of the treatment in any experimental groups; this could be due to the body's immunological regulation. All biochemical assay values were within normal ranges, as shown in Table **5.1**.

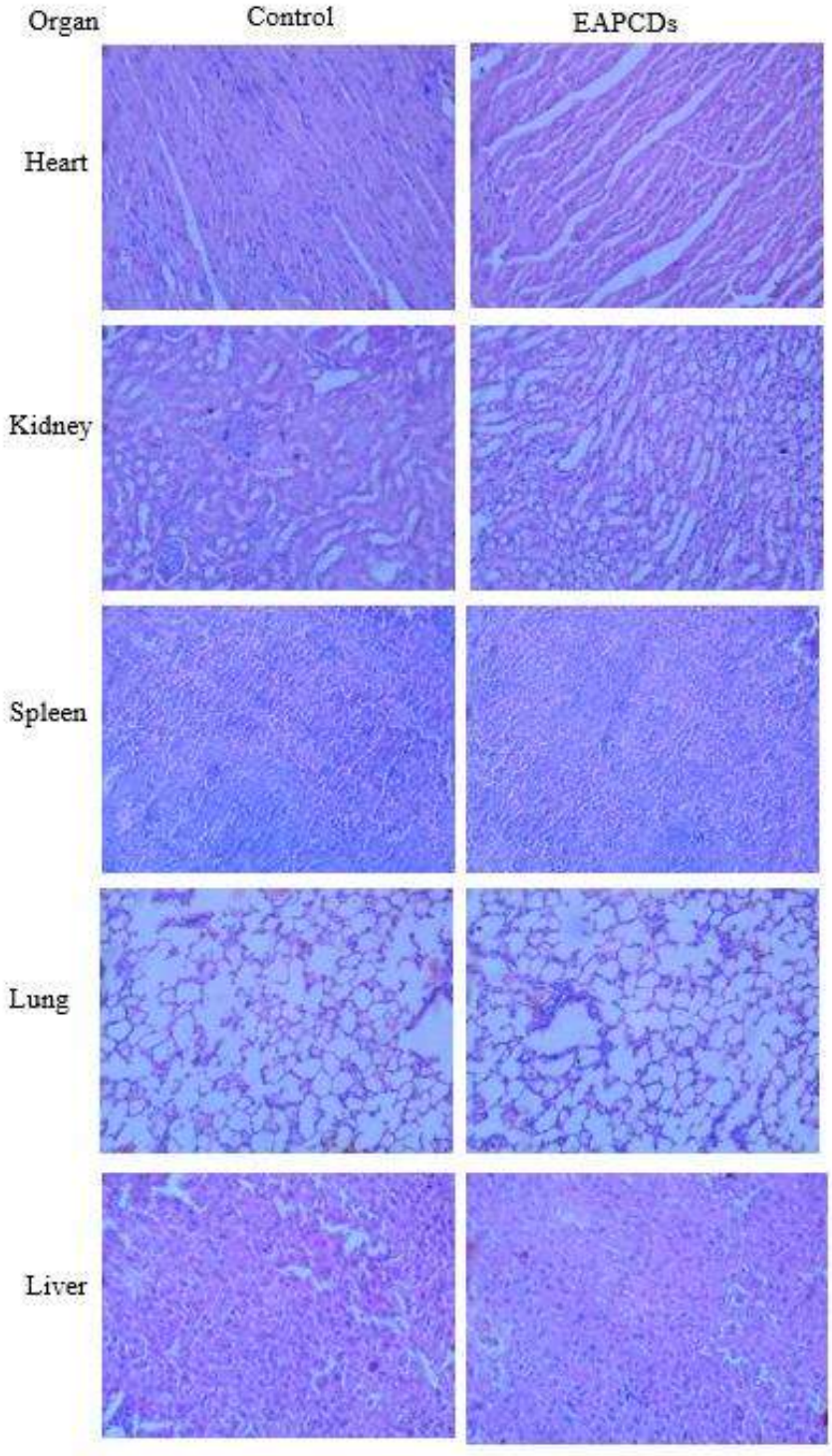

Figure 5.7. Histopathology of different mice organs treated with EAPCDs and control.

Hematology

Biochemical parameters such as alanine aminotransferase (ALT), creatinine (CRE), aspartate transaminase (AST), alkaline phosphatase (ALP), blood urea nitrogen (BUN), total bilirubin (TB), cholesterol, and creatine phosphokinase (CPK) were analyzed to measure organ toxicity as per standard protocols. Biochemical indicators, as shown in Table **5.1**, were within normal limits.

Table 5.1 Biochemical parameters of mice treated with EAPCDs and Control groups.

Parameters	**Normal Control**	**EAPCDs**
ALP (U/L)	105.13± 5.57	103.23± 5.28
AST(U/L)	134.46± 3.80	131.26± 3.87
ALT(U/L)	51.6± 1.75	53.1± 5.58
Creatinine (mg/dL)	0.23± 0.02	0.21± 0.01
Urea (mg/dL)	40.52± 3.86	44.21± 2.39
Cholesterol (mg/dL)	103± 5.09	102.33± 5.79
Tryglyceride (mg/dL)	106.53± 3.61	106.37± 4.52
Protein (g/dL)	6.39± 0.54	6.44± 0.56
Glucose (mg/dL)	140.93± 9.12	143.63± 3.73
CPK Total(U/L)	96.33± 5.24	99.66 ± 2.05

(Data was represented as mean± SD)

Peripheral blood was collected from mice post-treatment for hematological toxicity determination and subjected to several hematological parameters evaluation. All the

treatment groups and the normal control group's values were within the normal range (Table **5.2**), showing that the mice were not harmed by delivering EAPCDs nanoparticles.

Table 5.2 Hematological parameters of mice treated with EAPCDs and control groups.

Parameters	**Normal control**	**EAPCDs**
WBC (10^3/μL)	36.54±2.35	35.91±1.80
HGB (g/dL)	11.74±0.64	11.65±0.42
RBC (10^6/μL)	8.27±0.33	7.84±0.53
HCT (%)	36.12±1.40	36.22±0.86
MCV (fL)	45.69±1.03	45.66±1.39
MCH(pg)	14.38±0.21	14.40±0.16
NEUT (%)	55.80±2.94	52.93±4.53
LYM (%)	41.12±5.61	43.24±3.70
MONO (%)	3.76±0.33	3.55±0.13
EO (%)	0.80±0.03	0.83±0.04
BASO (%)	0.02±0.02	0.05±0.01

(Data was represented as mean± SD)

The histological investigation determined the microscopic interactions between CNDs and biological tissues. There were no evident histopathological changes in the heart, brain, kidney, spleen, lung, or liver observed compared to the control group. A histopathological examination revealed no signs of severe toxicity. These alterations could be attributable to environmental causes, like the mice in the control group exhibit

comparable symptoms. The cells and structure of these organs' samples were confirmed to be normal, and no specific lesion that differed from the control group was observed. The vital organs' H&E staining revealed the same characteristics as control sections.

On histological evaluation, the heart, kidney, brain, spleen, lung, and liver did not reveal any signs of toxicity, as shown in Figure **5.7**. In the test groups, no evident histological abnormalities or lesions were seen. The test group's cardiac muscle fibers were uniform and normal in shape and size.

The hepatocytes in the liver samples were normal, and no evidence of inflammation was seen. In the renal portion, the glomerulus structure was normal in texture. There was no evidence of necrosis in any of the histopathological samples examined. There was no steatosis, necrosis, or hydropic degeneration in the exposed hepatic sections. The liver lobule structure was normal, with only a few collagen fibers in the central vein and portal area. The red and white pulps were clear, and the splenic capsule was complete. The architecture of the lungs was normal, and no inflammation was discovered. The glomerular structure may be seen clearly in portions of the kidneys. Every other day, body weights were measured, and there were no differences between the experimental and control groups.

5.4 Conclusion

Fluorescent CNDs as a potential photomedicine were synthesized using a simple one-pot hydrothermal method. EAPCDs had a distinct pink fluorescence that was noticeable compared to previous reports. In terms of photochemical-optical properties and thermal stability, the CNDs performed admirably. For mercury sensing, a good linear relationship was obtained with a correlation coefficient (R2) of 0.996 for EAPCD with LOD=0.26 μM. Furthermore, these CNDs have low cytotoxicity at low doses but have cytotoxic effects on human breast carcinoma (MCF7) cells when the dose increases. At a concentration of 0.7 mg/mL EAPCDs, these cells were also nearly 50% viable. EAPCDs can rupture the membrane due to the high surface-to-volume ratio of CNDs and the small size of bacterial cells. Radiation scavenging and sensing abilities were also demonstrated by CNDs. We further tested the toxicity of these CNDs in swiss albino mice, and found that they were safe, as evidenced by biochemical, haematological, and histological parameters. Overall, EAPCDs as a photomedicine can be easily manufactured without harmful passivating agents, and they can be further investigated to open up more bio-analytical and pharmaceutical applications.